Environ. Sci. Technol. **2008,** *42,* 7496–7501

PCB Association with Model Phospholipid Bilayers

ANDREW S. CAMPBELL, YAN YU, STEVE GRANICK,* AND ANDREW A. GEWIRTH*

Department of Chemistry and Department of Materials Science and Engineering, University of Illinois, 600 S. Mathews Avenue, Urbana, Illinois 61801

Received April 22, 2008. Revised manuscript received July 1, 2008. Accepted July 8, 2008.

We compare the association of an ortho-substituted and a planar PCB (polychlorinated biphenyls PCB-52 and PCB-77, respectively) with single-component phospholipid bilayers terminated with phosphocholine headgroups. First, fluorescence correlation spectroscopy (FCS) studies of diffusion on supported fluid-phase DLPC show that the ortho-substituted PCB diffuses more slowly, indicating either complex formation or obstructed diffusion. Differential scanning calorimetry (DSC) of vesicles formed from DMPC shows that the gel-to-fluid phase transition temperature is lower for vesicles containing this ortho-substituted PCB. Atomic force microscopy (AFM) shows that, whereas supported bilayers of DMPC containing this ortho-substituted PCB display two melting points, bilayers containing the coplanar PCB display just a single melting point. A model is proposed in which the ortho-substituted PCB resides within the lipid tails of these phospholipid bilayers but the coplanar PCB associates preferentially with the headgroups. This model is consistent with the known membrane disruptive ability of the ortho substituted isomer.

Introduction

There is much interest in environmental contamination from persistent organic pollutants (POPs) due to their pervasiveness in the environment. Studies on the prevalence (*1, 2*) and remediation (*3*−*8*) of molecules such as polybrominated biphenyls (PBBs) and polychlorinated biphenyls (PCBs) provide evidence concerning the scope of the POP problem. Several studies on PBBs (*9*) and PCBs (*4, 10*−*16*) document their environmental persistence and propagation in fish and river sediments.

Different PCB isomers exhibit differing degrees of toxicity (*12*). Coplanar PCB congeners act on an aryl hydrocarbon (Ah) receptor, resulting in immune system suppression. However, PCB congeners substituted in positions ortho to the biphenyl bond are not coplanar and are too bulky to interact with the Ah receptor. Nonetheless, these ortho substituted congeners induce rapid cell death. The origin of this toxicity is the ability of the ortho PCB isomers to cause disruption of the cell membrane (*17*). Cyclosporin A, an agent which prevents channel opening in the mitochondria, prevents cell death upon ortho PCB exposure. Coplanar PCBs do not cause lipid disruption.

* Address correspondence to either author. Phone: 217-333-8329(A.A.G.), 217-333-5720(S.G.). Fax: 217-244-3186 (A.A.G.), 217-244-8544 (S.G.), E-mail: agewirth@uiuc.edu (A.A.G.), sgranick@uiuc.edu.

The origin of this different behavior has been examined by studies on cells and liposomes. Differences between ortho and planar PCBs have been examined by comparing the ortho substituted PCB 52 (2,2′,5,5′-tetrachlorobiphenyl) with the planar PCB 77 (3,3′,4,4′-tetrachlorobiphenyl). These studies show that cell death occurs rapidly following PCB 52 exposure but not upon exposure to PCB 77 (*12, 17*), and it has been conjectured that PCB 52 alters the cell membrane structure (*11*). However, a detailed physical picture of the interaction between different PCB isomers and bilayer membranes is not yet available, in part because the preponderance of work on these issues employs a mixture of PCB isomers (*18*) or utilizes cells with potentially complicated lipid, protein, and steroid interactions (*19, 20*). Studies on single component lipid structures can clarify the interaction of proteins and small molecules with the lipid bilayer structure (*21*−*29*).

Supported lipid bilayers present an approach to probe the interactions of molecules with lipid bilayer membranes of controlled structure and composition (*30*−*32*). Insight into topics as diverse as nanopore formation in a lipid bilayer following exposure to antimicrobial peptides (*33*), and proteins and cholesterol addition (*21, 34*−*36*), has been obtained. In this paper we examine the interaction of PCBs 52 and 77 with supported lipid bilayers. FCS with single-molecule sensitivity is used to measure the diffusion of phosphocholine lipids in a supported bilayer with and without PCBs. In addition, DSC of vesicles interrogates the magnitude of membrane insertion for PCB-incorporated phosphocholine bilayers. Magnetic-acoustic mode AFM is employed to visualize the phase transition of supported phospholipid bilayers with each PCB congener incorporated into the membrane. Taken together, these studies motivate a tentative model for the mechanism of PCB−lipid association.

Experimental Section

All solutions were prepared using ultrapure water (18.2 MΩ cm, Milli-Q UV Plus, Millipore, Billerica, MA). A 10 mM, pH 6.0 phosphate buffer solution (PBS) was prepared from Na_2HPO_4 and $NaH_2PO_4 \cdot H_2O$ (99.9%, Sigma). 1,2-dimyristoyl-*sn*-glycero-3-phosphocholine (DMPC), 1,2-dilauroyl-*sn*-glycero-3-phosphocholine (DLPC), and rhodamine-labeled 1,2-dimyristoyl-*sn*-glycero-3-phosphoethanolamine (DMPE) were purchased from Avanti Polar Lipids, Inc. (Alabaster, AL) and used without further purification. PCB no. 52 and PCB no. 77 (structures shown in the Supporting Information) were purchased from Sigma-Aldrich (Milwaukee, WI) and Ultra Scientific (North Kingstown, RI). Chloroform (99.9%, Fisher) was used to prepare stock lipid solutions. Sample preparation procedures are included in the Supporting Information.

FCS measurements were obtained using a home-built instrument as described previously (*37*). Two-photon excitation at the diffraction-limited focus of a laser beam enabled measurements that were spatially resolved. Near-infrared light from a femtosecond Ti:Sapphire laser (800 nm, 82 MHz, pulse width ∼100 fsec) was focused onto the sample through a water immersion objective lens (Zeiss Axiovert 135 TV, x63, numerical aperture 1.2). Fluorescence was excited only at the focus, giving an excitation spot whose diffraction-limited diameter was ∼0.35 μm. Fluorescence was collected through the same objective and detected by a single photon counting module (Hamamatsu, Middlesex, NJ). The 10 ppm concentration of fluorescent rhodamine-labeled DMPE was selected such that on average one sole fluorescent molecule resided within the area sampled. Additional measurements of PCBs

10.1021/es8011063 CCC: $40.75

Published on Web 08/22/2008

in unlabeled DLPC bilayers were made to observe diffusion of the PCB molecules. In deducing the diffusion coefficients presented below, each is the average of 10−20 experiments performed at different locations on the surface.

DSC was performed on a Mettler-Toledo DSC 821e, calibrated by indium, octane, and zinc standards. Unless otherwise indicated, the heating rate was 1.5 °C·min^{-1}. For each analysis, approximately 10−20 mg of sample were weighed (±0.02 mg) into an aluminum pan, which was hermetically sealed. DSC traces recorded heat flow during a heating, cooling, and heating cooling cycle over the temperature range of 10−40 °C.

Atomic force micrographs were obtained using a PicoSPM 300 (Molecular Imaging, Tempe, AZ) with a type D scanner controlled with a Nanoscope E controller (Digital Instruments, Houston, TX) in magnetic-acoustic mode. The natural resonance frequency of the cantilever was 22−25 kHz in aqueous solution, and the spring constant was 2.8 N/m. Images were collected with a scan rate of 2 Hz. Temperature control was realized using a 1 × Peltier sample stage (Molecular Imaging) and controlled with a model 311 temperature controller (Lake Shore Cryotronics, Cleveland, OH). The stage was cooled using a gravity-fed ice-water bath. For heating and cooling, temperatures were ramped 0.3 °C per minute and were allowed to equilibrate 5 min before capturing images.

Results

In all experiments, the PCB concentration was 7.2 μm unless otherwise noted. This concentration was selected based on PCB concentration in similar studies (*11, 17*). In interpreting the findings, we were sensitive to the possibility that differences in the behavior of the two PCB isomers might relate to different extents of partitioning with the lipid. To test this possibility, a sample of PCB 52 in DMPC was injected into a dialysis cassette and dialyzed twice with 200 mL of pH 6 PBS for 2 and 5 h, respectively and both buffers and a chloroform extract of the dialysis membrane were analyzed by UV−vis. A standard curve of PCB 52 demonstrated that the concentration of PCB 52 in each of the extracts was within baseline noise, and the same result was found for a sample of PCB 77 in DMPC vesicles under identical conditions; these control experiments indicate that virtually all PCB molecules became incorporated into the lipid vesicles. Additional partition coefficient measurements show that the K_P of both PCB 52 and PCB 77 is on the order of 10^5. Thus, differences between PCB 52 and PCB 77 do not appear to stem from differences in their partitioning to the bilayers.

Fluorescence Correlation Spectroscopy. An autocorrelation curve (Supporting Information) was obtained from FCS measurements of a supported DLPC bilayer containing 0.001% rhodamine-DMPE without PCB, with PCB 52, and with PCB 77. DLPC and DMPE were used in place of DMPC because of their lower average melting temperature, which allowed us to observe fluid phase diffusion in the bilayer. The autocorrelation curves were fit to eq 1 (*38, 39*) by using a nonlinear least-squares method.

$$G(\tau) = \left(\frac{2}{\pi w^2 c}\right)\left(\frac{f_1}{\frac{1+8D_1\tau}{w^2}} + \frac{1-f_1}{\frac{1+8D_2\tau}{w^2}}\right) + B \qquad (1)$$

Equation 1 relates the autocorrelation function $G(\tau)$ at time interval τ to the width of the focus volume (w), the concentration of fluorescent molecules (c), the diffusion coefficient(s) (D_1 and D_2), the fraction of diffusing component 1 in total diffusing components (f_1), and the baseline (B). In fitting the autocorrelation curves, w is set based on a calibration, here, 0.35 μm, which is the diffraction-limited diameter of the focused laser beam.

In all measurements with PCB-containing samples, the best fit of the autocorrelation data to eq 1 yielded two diffusion coefficients, indicating the presence of two distinct diffusing species. Values of the diffusion coefficients are listed in Table 1 and have an uncertainty of about 20% owing to the difficulty of two-component fitting. In Table 1, D_1 is the first diffusion coefficient for samples prepared with rhodamine-labeled lipid, whereas D_1' is the first diffusion coefficient for samples prepared absent rhodamine-labeled lipid. D_2 is the second diffusion coefficient in all samples.

Table 1 shows that the first diffusion coefficient obtained from the rhodamine-labeled lipid samples (D_1) is the typical diffusion coefficient for supported DLPC bilayer in fluid phase (*40*) and essentially independent of the presence or absence of PCB. This suggests that morphology of the bilayer remains intact after PCB adsorbs.

FCS measurements of the adsorbed PCB itself were enabled by the fact that both PCBs exhibit weak fluorescence upon two-photon excitation at 800 nm. The maximum of absorbance for both PCBs is at 264 nm with weak tails around 400 nm where the two-photon excitation occurs (*20*). Fits to the resulting autocorrelation curves (not shown) gave two diffusion coefficients. For the ortho isomer the faster component is similar in magnitude to the fast component measured for dye-labeled lipid, but for the coplanar isomer the faster component is a factor of 2 even faster, suggesting even weaker association with the bilayer (to which we return in the model proposed below). However, for both PCBs the slower diffusion coefficients (D_2) coincide within experimental uncertainty with the slower component measured for dye-labeled lipid in the presence of these same PCBs.

Differential Scanning Calorimetry. Figure 1 shows the results of differential scanning calorimetry obtained from DMPC vesicles without PCB added (A), DMPC vesicles with PCB 77 added (B), and DMPC vesicles with PCB 52 added (C). A negligible shift in phase transition temperature from 22.8 to 22.6 °C is seen when PCB 77 is added to the vesicles. A more significant reduction in transition temperature is observed when the same amount of PCB 52 is added to the vesicles, from 22.8 to 18.4 °C.

Enthalpies of transition for each thermogram can be calculated by using eq 2.

$$\Delta H = KA \qquad (2)$$

TABLE 1. Diffusion Coefficients Inferred from FCS Measurements on Supported Lipid Bilayers of DLPC[a]

sample description	$D_1/\mu m^2 s^{-1}$	$D_1'/\mu m^2 s^{-1}$	$D_2/\mu m^2 s^{-1}$
labeled DLPC	3.0 ± 0.3		
PCB 52 in labeled DLPC	2.8 ± 1.6		0.12 ± 0.07
PCB 52 in unlabeled DLPC		3.2 ± 1.2	0.07 ± 0.03
PCB 77 in labeled DLPC	3.4 ± 1.3		0.42 ± 0.17
PCB 77 in unlabeled DLPC		8.6 ± 3.5	0.32 ± 0.24

[a] D_1 is the first diffusion coefficient for samples prepared with rhodamine-labeled lipid, whereas D_1' is the first diffusion coefficient for samples prepared absent rhodamine-labeled lipid. D_2 remains the second diffusion coefficient in all samples.

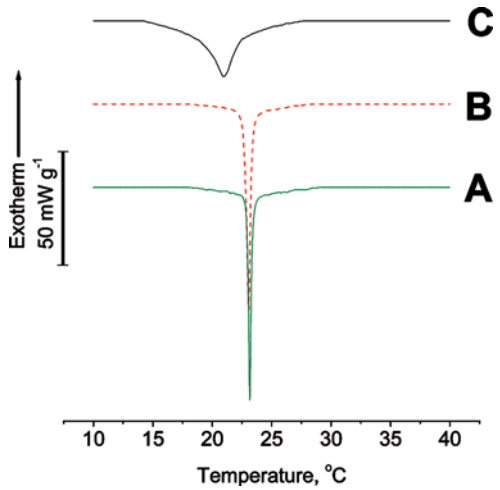

FIGURE 1. Differential scanning calorimetry (DSC) thermograms of (A) DMPC (dotted line), (B) PCB 77 in DMPC (22% w/w, dashed line), and (C) PCB 52 in DMPC (23% w/w, solid line). The enthalpies of fusion, ΔH_{fus}, are 1.29, 1.81, and 3.55 J·g^{-1} for these three cases, respectively.

Here K is the calorimetric constant of the instrument and A is the area of the transition peak. The thermogram of PCB 77 in DMPC vesicles shows a small increase in ΔH_{fus} from 1.29 ± 0.06 to 1.81 ± 0.09 J·g^{-1}. However, PCB 52 in DMPC vesicles shows peak broadening and an increase in ΔH_{fus} from 1.29 ± 0.06 to 3.55 ± 0.18 J·g^{-1}. Peak broadening in DSC often reflects presence of an impurity (*41*). The fact that broadening is not observed with PCB 77 could signify that it does not associate as strongly with the lipid bilayer.

Changes in ΔH and T_m in response to the presence of other PCB mixtures in other phospholipid liposomes have been correlated to polarity and charge distribution in the lipid headgroups, although those studies do not address the influence of the different PCB isomers studied here (*18*). Our data shows that identical lipids exhibit differences in transition behavior when different PCB isomers at the same concentration are introduced.

Atomic Force Microscopy. The consequences of PCB insertion in the lipid bilayer can also be visualized using AFM, building on a prior study of the phase transition of DMPC (*42*). Figure 2 shows the gel to fluid phase transition of a supported DMPC bilayer incubated with PCB 77. Below the melting temperature, cracks associated with the initial stages of the phase transition are observed, and these continue growing in breadth until the entire image range is one phase height at 28 °C. Higher temperatures brought no change in image appearance. During this sequence, defect holes generated during the transition from the fluid phase to the denser gel phase became filled by the mobile liquid-phase lipids. The defect features highlighted in the dashed boxes in Figure 2 most clearly illustrate the completion from gel to fluid phase. The morphology of the cracks is consistent with that observed during the first phase transition of a PCB-free DMPC bilayer (*42*). However, unlike the PCB-free case, only one phase transition is observed. We previously saw that incubating the DMPC bilayer with gramicidin, a leaflet bridging protein, also results in removal of the second phase transition, associated with the different environments seen by the top and bottom bilayer leaflets (*42*).

Figure 3 shows the gel to fluid phase transition from a supported DMPC bilayer incubated with PCB 52. Several differences relative to the PCB 77 case are observed. At 13 °C, the initial stages of the phase transition are already seen, as expected from the DSC results. The bilayer height is on average 5.2 nm. As the temperature increases, cracks increase in size and major defects are filled in by fluid phase lipid. This continues to about 22−23 °C, where cracking ceases and only one phase along with small defects is seen.

As the temperature is raised to 32 °C, a second phase transition is observed and the consequences of this transition persist until temperatures as high as 47 °C are reached. At this point, the entire image scan area is filled with one uniform liquid-phase lipid.

The presence of a second phase transition is also seen in PCB-free bilayers. However, the phase transition in the presence of PCB 52 occurs over a much larger temperature range (13−45 °C) relative to the PCB-free case (22−31 °C) (*42*).

Discussion

The results presented above show changes in the diffusion coefficient, enthalpy of transition, and bilayer morphology during gel-to-fluid phase transition behavior, all differ

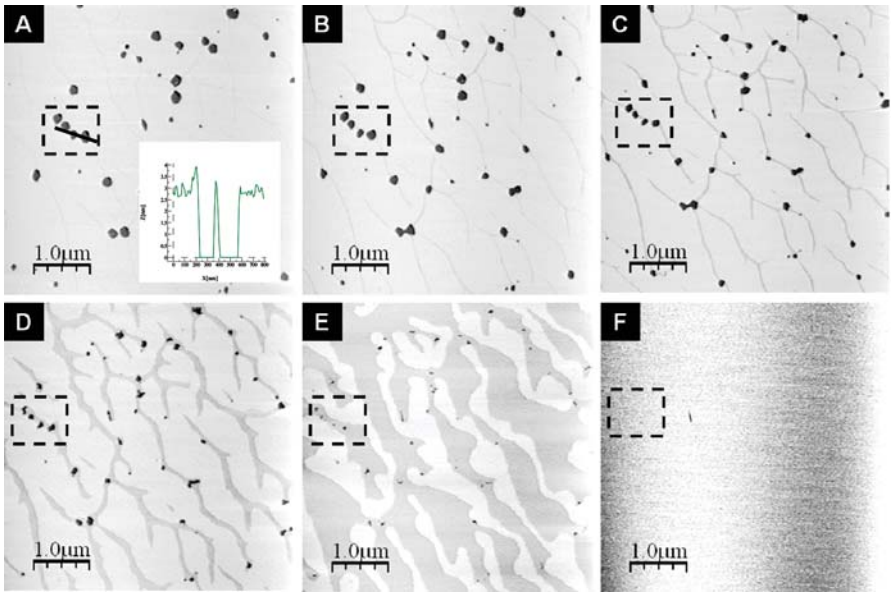

FIGURE 2. Atomic force microscopy (AFM) measurements of bilayer morphology for PCB 77 in supported DMPC bilayers at (A) 15 °C, (B) 18 °C, (C) 21 °C, (D) 23 °C, (E) 25 °C, and (F) 28 °C. Note the defect filling in the dashed boxes during the transition. Figure 2A inset shows cross-section of boxed defects with an average depth of 3.5 nm (*45*).

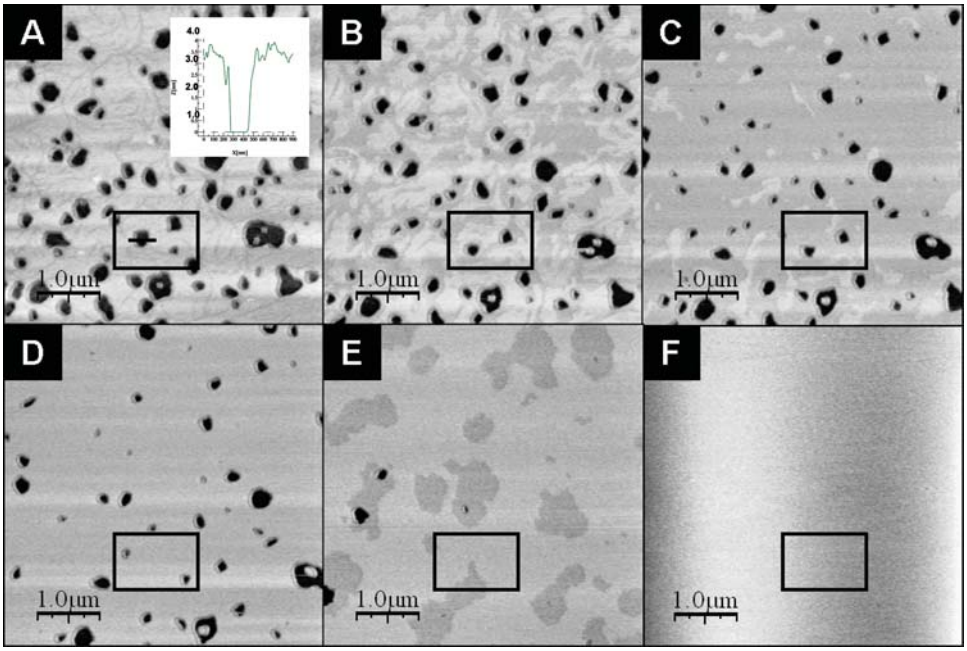

FIGURE 3. Atomic force microscopy (AFM) measurements of bilayer morphology for PCB 52 in supported DMPC bilayers at (A) 14 °C, (B) 18 °C, (C) 20 °C, (D) 22 °C, (E) 32 °C, and (F) 47 °C. Note the defect filling and patch growth in the solid boxes during the transition. Figure 3A inset shows cross-section of boxed defects with an average depth of 3.0 nm (*45*).

according to whether the bilayer was exposed to an ortho or coplanar isomer of PCB. The FCS experiments, showing that the complex with the ortho isomer diffuses a factor of 2 more slowly than that with the coplanar isomer, suggests a tighter interaction in the former case. It is also notable that the uncomplexed PCB, quantified by D_1' values in Table 1) is also lower for the ortho (PCB 52) sample and that D_1' for the coplanar (PCB 77) sample is faster than that of the lipid itself. These findings signify either that the PCB-lipid interaction is stronger in the case of the ortho PCB, or that the environment, in the case of the coplanar isomer, provides less impediment to diffusion. These observations are consistent with the calorimetry experiments, showing that the enthalpy of melting is increased for bilayers containing ortho PCB 52 but not coplanar PCB 77. Peak broadening, observed in the thermogram of the former only, also suggests greater disruption of the lipid bilayer by this PCB isomer.

Turning to the AFM measurements of bilayer morphology, we note that while both bilayers have similar morphology at low temperature and that the average height of both bilayers is about 4.5 nm, the bilayer incorporating the ortho isomer has a start and end temperature about 4 °C lower for the first phase transition, compared with the first transition of a PCB-free bilayer. Another particularly interesting feature of bilayers containing the ortho isomer is the extended presence of "patches," an intermediate phase domain (Figure 3E, for example). In Figure 2E, this lower liquid phase domain covers 34% of the surface area, whereas the higher gel phase domain covers 66% of the area. This domain is present from as low as 31 °C and grows until 47 °C, at which point a uniform, liquid phase morphology is observed. Bilayers containing the same concentration of the coplanar isomer (Figure 2) or without added PCB complete this transition at lower temperatures. Also, when making comparisons at the same temperature, the size of defects in this type of bilayer are larger. Taken together, these observations show that presence of the ortho PCB isomer stabilizes the gel phase to higher temperatures.

Seeking interpretation of these differences on the molecular level, we first consider the dipole moment of these two PCB isomers. The dipole moment of the ortho isomer is zero, by symmetry, but that of the coplanar isomer (PCB 77) is calculated to be substantial, 3.07 D (calculation performed using Spartan ver. 1.0.2 (Wave function, Inc., 2006)). This difference may influence preferential location of each PCB isomer in the bilayer. A more polarizable molecule may associate preferentially with the polar phospholipid headgroup, whereas the isomer with zero dipole moment may associate preferentially with the hydrophobic tails.

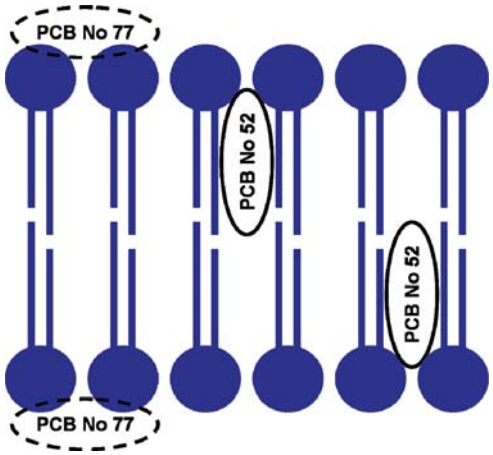

FIGURE 4. Proposed model of PCB-lipid bilayer interactions examined in this study.

We note further that the ortho isomer (PCB 52) is bulkier, as one notices when considering torsional angles of the two PCBs investigated here. For the coplanar isomer, whose chlorine atoms are located farther from the biphenyl, the torsional angle is 37.7°, but for the ortho isomer it is 81.3° (*43*). The thinner coplanar isomer (PCB 77) might insert more easily into the bilayer.

Based on these considerations, Figure 4 depicts tentative proposed interactions of each PCB with the bilayers: the ortho PCB interacts preferentially with the lipid interior and the coplanar isomer interacts preferentially with the polar headgroups. Cholesterol exerts a similar diffusion-inhibiting effect when inserted into bilayers (*44*). The model implies that the ortho isomer may tend to orient parallel to bilayers

and the coplanar isomer perpendicular to them, but this data is not available at the present time. This model is consistent with all of the main differences in physical behavior summarized in this study. In particular, as in this model the coplanar isomer does not insert into bilayers, it does not specifically disrupt their structure, does not lead to retarded diffusion of complexes with lipids, and does not significantly perturb the melting point. The degree to which the stronger influence of the ortho (PCB 52) isomer might reflect stronger binding, or might simply involve disruption of local packing owing to the irregular shape, is not clear at the present time. Toxicology studies by others on these PCB isomers show that they are toxic for different reasons. While PCB 77 acts on the Ah receptor, PCB 52 toxicity arises from membrane disruption, which is consistent with the model in Figure 4.

Acknowledgments

We thank Professor Jeffrey Moore for use of a differential scanning calorimeter and Professor Kenneth Suslick for use of a UV−vis spectrophotometer. A.S.C. gratefully acknowledges support through a J. C. Bailar Fellowship. This work was supported by the National Science Foundation. S.G. and Y.Y. were supported by the Department of Energy, Division of Materials Science, under Award No. DEFG02-02ER46019, and acknowledge equipment support from NSF-DMR-06-05947.

Supporting Information Available

Table S1. This material is available free of charge via the Internet at http://pubs.acs.org.

Literature Cited

(1) Carroll, J.; Savinov, V.; Savinova, T.; Dahle, S.; McCrea, R.; Muir, D. C. G. PCBs, PBDEs and pesticides released to the Arctic Ocean by the Russian Rivers Ob and Yenisei. *Environ. Sci. Technol.* **2008**, *42* (1), 69–74.

(2) Loganathan, B. G.; Kumar, K. S.; Masunaga, S.; Sajwan, K. S. Polychlorinated Dibenzo-p-Dioxins, Dibenzofurans, and Dioxin-Like Polychlorinated Biphenyls in Sediment and Mussel Samples from Kentucky Lake, USA. *Arch. Environ. Contam. Toxicol.* **2008**, *54* (1), 20–30.

(3) Sawatsubashi, T.; Tsukahara, C.; Baba, K.; Ohi, E.; Shinoda, A.; Miura, N. Development of new-type rapid analysis technology of polychlorinated biphenyls by using liquid chromatographic clean-up material (polyvinyl alcohol gel). *J. Chromatogr., A.* **2008**, *1177* (1), 138–149.

(4) Adebusoye, S. A.; Ilori, M. O.; Picardal, F. W.; Amund, O. O. Cometabolic degradation of polychlorinated biphenyls (PCBs) by axenic cultures of Ralstonia sp. strain SA-5 and Pseudomonas sp. strain SA-6 obtained from Nigerian contaminated soils. *World J. Microbiol. Biotechnol.* **2008**, *24* (1), 61–68.

(5) Matykiewiczova, N.; Klanova, J.; Klan, P. Photochemical degradation of PCBs in snow. *Environ. Sci. Technol.* **2007**, *41* (24), 8308–8314.

(6) Vasilyeva, G. K.; Strijakova, E. R. Bioremediation of soils and sediments contaminated by polychlorinated biphenyls. *Microbiology (Road Town, Virgin Islands (British))* **2007**, *76* (6), 639–653.

(7) Przado, D.; Kafarski, P.; Steininger, M. Studies on degradation of polychlorinated biphenyls by means of Fenton's reagent. *Pol. J. Environ. Stud.* **2007**, *16* (6), 881–887.

(8) Bhowmik, S.; Horsman, G. P.; Bolin, J. T.; Eltis, L. D. The molecular basis for inhibition of BphD, a C-C bond hydrolase involved in polychlorinated biphenyls degradation: Large 3-substituents prevent tautomerization. *J. Biol. Chem.* **2007**, *282* (50), 36377–36385.

(9) Kammann, U.; Vobach, M.; Wosniok, W. Toxic effects of brominated indoles and phenols on zebrafish embryos. *Arch. Environ. Contam. Toxicol.* **2006**, *51* (1), 97–102.

(10) Bachour, G.; Failing, K.; Georgii, S.; Elmadfa, I.; Brunn, H. Species and organ dependence of PCB contamination in fish, foxes, roe deer, and humans. *Arch. Environ. Contam. Toxicol.* **1998**, *35* (4), 666–673.

(11) Tan, Y.; Chen, C.-H.; Lawrence, D.; Carpenter, D. O. Ortho-substituted PCBs kill cells by altering membrane structure. *Toxicol. Sci.* **2004**, *80* (1), 54–59.

(12) Tan, Y.; Li, D.; Song, R.; Lawrence, D.; Carpenter, D. O. Ortho-substituted PCBs kill thymocytes. *Toxicol. Sci.* **2003**, *76* (2), 328–337.

(13) Adebusoye, S. A.; Picardal, F. W.; Ilori, M. O.; Amund, O. O.; Fuqua, C. Characterization of multiple novel aerobic polychlorinated biphenyl (PCB)-utilizing bacterial strains indigenous to contaminated tropical African soils. *Biodegradation* **2008**, *19* (1), 145–159.

(14) Fuchsman, P. C.; Barber, T. R.; Bock, M. J. Effectiveness of various exposure metrics in defining dose-response relationships for mink (mustela vison) exposed to polychlorinated biphenyls. *Arch. Environ. Contam. Toxicol.* **2008**, *54* (1), 130–144.

(15) Moeckel, C.; Thomas, G. O.; Barber, J. L.; Jones, K. C. Uptake and storage of PCBs by plant cuticles. *Environ. Sci. Technol.* **2008**, *42* (1), 100–105.

(16) Yang, F.; Xu, Y.; Pan, H.; Wu, D. Induction of hepatic cytochrome P4501A1/2B activity and disruption of thyroglobulin synthesis/secretion by mono-ortho polychlorinated biphenyl and its hydroxylated metabolites in rat cell lines. *Environ. Toxicol. Chem.* **2008**, *27* (1), 220–225.

(17) Tan, Y.; Song, R.; Lawrence, D.; Carpenter, D. O. Ortho-substituted but not coplanar PCBs rapidly kill cerebellar granule cells. *Toxicol. Sci.* **2004**, *79* (1), 147–156.

(18) Bonora, S.; Torreggiani, A.; Fini, G. DSC and Raman study on the interaction between polychlorinated biphenyls (PCB) and phospholipid liposomes. *Thermochim. Acta* **2003**, *408* (1−2), 55–65.

(19) Carpenter, D. O.; Stoner, C. R. T.; Lawrence, D. A. Flow cytometric measurements of neuronal death triggered by PCBs. *Neurotoxicology* **1997**, *18* (2), 507–513.

(20) Oakley, G. G.; Robertson, L. W.; Gupta, R. C. Analysis of polychlorinated biphenyl - DNA adducts by 32P-postlabeling. *Carcinogenesis* **1996**, *17* (1), 109–14.

(21) Yuan, B.; Xing, L.-L.; Zhang, Y.-D.; Lu, Y.; Luo, Y.-Y.; Mai, Z.-H.; Li, M. Penetration and saturation of lysozyme in phospholipid bilayers. *J. Phys. Chem. B* **2007**, *111* (22), 6151–6155.

(22) Bonora, S.; Ercoli, L.; Torreggiani, A.; Fini, G. Influence of sebacate plasticizers on the thermal behaviour of dipalmitoylphosphatidylcholine liposomes. *Thermochim. Acta* **2002**, *385* (1−2), 51–61.

(23) Cacela, C.; Hincha, D. K. Low amounts of sucrose are sufficient to depress the phase transition temperature of dry phosphatidylcholine, but not for lyoprotection of liposomes. *Biophys. J.* **2006**, *90* (8), 2831–2842.

(24) Feng, Z. V.; Granick, S.; Gewirth, A. A. Modification of a supported lipid bilayer by polyelectrolyte adsorption. *Langmuir* **2004**, *20* (20), 8796–8804.

(25) Frey, S. L.; Lee, K. Y. C. Temperature dependence of poloxamer insertion into and squeeze-out from lipid monolayers. *Langmuir* **2007**, *23* (5), 2631–2637.

(26) Luxnat, M.; Galla, H. J. Partition of chlorpromazine into lipid bilayer membranes: The effect of membrane structure and composition. *Biochim. Biophys. Acta, Biomembranes* **1986**, *856* (2), 274–82.

(27) Spurlin, T. A.; Gewirth, A. A. Poly-L-lysine-induced morphology changes in mixed anionic/zwitterionic and neat zwitterionic-supported phospholipid bilayers. *Biophys. J.* **2006**, *91* (8), 2919–2927.

(28) Varga, Z.; Bota, A.; Goerigk, G. Localization of dibromophenol in DPPC/water liposomes studied by anomalous small-angle X-ray scattering. *J. Phys. Chem. B* **2006**, *110* (23), 11029–11032.

(29) Chiantia, S.; Kahya, N.; Schwille, P. Raft domain reorganization driven by short- and long-chain ceramide: A combined AFM and FCS study. *Langmuir* **2007**, *23* (14), 7659–7665.

(30) Chan, Y.-H. M.; Boxer, S. G. Model membrane systems and their applications. *Curr. Opin. Chem. Biol.* **2007**, *11* (6), 581–587.

(31) Castellana, E. T.; Cremer, P. S. Solid supported lipid bilayers: From biophysical studies to sensor design. *Surf. Sci. Rep.* **2006**, *61* (10), 429–444.

(32) Sackmann, E., Supported membranes: scientific and practical applications. *Science* 1996, *271*, (5245), 43−8.

(33) Lam, K. L. H.; Ishitsuka, Y.; Cheng, Y.; Chien, K.; Waring, A. J.; Lehrer, R. I.; Lee, K. Y. C. Mechanism of Supported membrane disruption by antimicrobial peptide protegrin-1. *J. Phys. Chem. B* **2006**, *110* (42), 21282–21286.

(34) Zuckermann, M. J.; Heimburg, T. Insertion and pore formation driven by adsorption of proteins onto lipid bilayer membrane-water interfaces. *Biophys. J.* **2001**, *81* (5), 2458–2472.

(35) Doyle, A. W.; Fick, J.; Himmelhaus, M.; Eck, W.; Graziani, I.; Prudovsky, I.; Grunze, M.; Maciag, T.; Neivandt, D. J. Protein deformation of lipid hybrid bilayer membranes studied by sum

frequency generation vibrational spectroscopy. *Langmuir* **2004**, *20* (21), 8961–8965.
(36) Pike, L. J. Lipid rafts: Bringing order to chaos. *J. Lipid Res.* **2003**, *44* (4), 655–667.
(37) Zhao, J. J.; Bae, S. C.; Xie, F.; Granick, S. Diffusion of polymer-coated nanoparticles studied by fluorescence correlation spectroscopy. *Macromolecules* **2001**, *34* (10), 3123–3126.
(38) Rigler, R.; Elson, E. S., *Fluorescence Correlation Spectroscopy: Theory and Application*; Springer: Berlin, 2001.
(39) *Fluorescence Correlation Spectroscopy (FCS) Technical Manual*. ISS: Champaign, IL, 2000; Vol. *10/30/00*.
(40) Zhang, L.; Granick, S. Lipid diffusion compared in outer and inner leaflets of planar supported bilayers. *J. Chem. Phys.* **2005**, *123* (21), 211104/1–211104/4.
(41) Brown, M. E., *Introduction to Thermal Analysis: Techniques and Applications* 2nd ed.; Kluwer Academic Publishers: Boston, 2001.
(42) Feng, Z. V.; Spurlin, T. A.; Gewirth, A. A. Direct visualization of asymmetric behavior in supported lipid bilayers at the gel-fluid phase transition. *Biophys. J.* **2005**, *88* (3), 2154–2164.
(43) Dorofeeva, O. V.; Novikov, V. P.; Moiseeva, N. F.; Yungman, V. S. Density functional theory study of conformations, barriers to internal rotations and torsional potentials of polychlorinated biphenyls. *Theochem* **2003**, *637*, 137–153.
(44) Filippov, A.; Oradd, G.; Lindblom, G. Influence of cholesterol and water content on phospholipid lateral diffusion in bilayers. *Langmuir* **2003**, *19* (16), 6397–6400.
(45) Horcas, I.; Fernandez, R.; Gomez-Rodriguez, J. M.; Colchero, J.; Gomez-Herrero, J.; Baro, A. M. WSXM: a software for scanning probe microscopy and a tool for nanotechnology. *Rev. Sci. Instrum.* **2007**, *78* (1), 013705/1–013705/8.

ES8011063